MIT Libraries | DSpace@MIT

MIT Open Access Articles

Yield Hardening of Electrorheological Fluids in Channel Flow

Massachusetts Institute of Technology

Yield Hardening of Electrorheological Fluids in Channel Flow

Ahmed Helal,[*] Bian Qian, Gareth H. McKinley, and A. E. Hosoi

Department of Mechanical Engineering, Hatsopoulos Microfluids Laboratory,
Massachusetts Institute of Technology, 77 Massachusetts Avenue, Cambridge, Massachusetts 02139, USA

Electrorheological fluids offer potential for developing rapidly actuated hydraulic devices where shear forces or pressure-driven flow are present. In this study, the Bingham yield stress of electrorheological fluids with different particle volume fractions is investigated experimentally in wall-driven and pressure-driven flow modes using measurements in a parallel-plate rheometer and a microfluidic channel, respectively. A modified Krieger-Dougherty model can be used to describe the effects of the particle volume fraction on the yield stress and is in good agreement with the viscometric data. However, significant yield hardening in pressure-driven channel flow is observed and attributed to an increase and eventual saturation of the particle volume fraction in the channel. A phenomenological physical model linking the densification and consequent microstructure to the ratio of the particle aggregation time scale compared to the convective time scale is presented and used to predict the enhancement in yield stress in channel flow, enabling us to reconcile discrepancies in the literature between wall-driven and pressure-driven flows.

I. INTRODUCTION

Electrorheological (ER) fluids are materials that exhibit a reversible change in rheological properties with the application of an external electric field [1]. They consist, typically, of a suspension of dielectric particles in an insulating carrier fluid. When an electric field is applied, the particles aggregate and align in the direction of the field, forming columns consisting of chains of particles, which cause the fluid to transition from a liquidlike to a soft solidlike state. This change in the fluid properties is very rapid (on the order of tens of milliseconds) and is reversible upon removal of the electric field. These features make ER fluids promising candidates for use in a variety of hydraulic components and microfluidic devices including valves, clutches, and dampers. Devices based on ER fluids can operate under three different modes: shear, flow, and squeeze [2]. In shear mode, one of the electrodes is free to move in its plane, and common applications include clutches, brakes, and dampers [3]. In flow mode, the electrodes are fixed, and the pressure drop across the channel is controlled using the electric field. Valves and vibrators are typical applications in which ER fluids are used in flow mode [4–6]. In squeeze mode, the electrode gap is varied, and the fluid is compressed in the wall-normal direction. Vibration control, shock absorbers, and dampers are examples of application of ER fluids used in squeeze mode [2,3]. A summary of the different modes of operation and their typical engineering applications is shown in Table I. For each mode of operation, the particle interaction and the particle structures that are

formed affect the mechanical properties of the ER fluid, most notably, its yield strength. Thus, an understanding of the microstructures that form is crucial to predicting the mechanical performance of devices utilizing ER fluids. In shear mode, shear-induced lamellar structures are known to form, while in flow mode, the suspension microstructure tends to contain clusters and aggregates [7–9]. In addition, an enhancement in the shear yield strength has been shown in magnetorheological fluids as the fluid is compressed in the direction orthogonal to shear [10] and a strengthening of the microstructure of ER fluids has also been shown in squeeze mode by Tian *et al.* [11].

The rheological response of ER fluids under shear is traditionally modeled using a continuum approach with a Bingham plastic model, where the application of the field induces a field-dependent yield stress [4]. The rheological constitutive relation for the ER fluid is typically expressed as

TABLE I. A summary of the different modes of operation of ER devices and their typical engineering applications.

Mode of operation	Illustrative schematic	Applications
Shear mode		Clutches, brakes, dampers [2,3]
Flow mode		Valves, vibrators [2–6]
Squeeze mode		Shock absorbers, dampers [2,3]

[*]ahelal@mit.edu

$$\dot{\gamma} = 0 \quad \text{if } \tau < \tau_y(E, \phi),$$
$$\tau = \tau_y + \mu\dot{\gamma} \quad \text{if } \tau > \tau_y(E, \phi), \quad (1)$$

where τ is the shear stress, $\dot{\gamma}$ the shear rate, μ the plastic viscosity, $\tau_y(E, \phi)$ is the field-dependent yield stress, E the electric field, and ϕ the particle volume fraction. ER fluid applications, in both shear and flow modes, have been successfully modeled using Eq. (1), and it has been demonstrated that experimental results align well with this model [12–14].

For regular yield stress fluids, knowledge of the rheological constitutive relation in one mode can be used to predict the flow performance in a different mode. However, recent studies [12,15,16] indicate that there is a difference in the dynamic response of ER fluids in shear and flow modes. Lee and Choi [12] have compared the rheological properties of an ER fluid in both modes and observed that the Bingham yield stress is higher in flow mode. Nam *et al.* [15] have studied the dynamic response of an ER fluid in steady pressure-driven flow and found that the response in flow mode is dominated by a densification process in which the competition between particle interaction and hydrodynamic forces on the incoming particles leads to cluster formation. On the other hand, in shear mode, they note that the aggregation of chains into columns is the dominant process. This is in agreement with recent studies by Qian *et al.* [17] on structure evolution in channel flow of ER fluids.

In order to accurately model systems which utilize ER fluids, particularly ER valves, there is a need for a better understanding of how the yield-hardening behavior observed in channel flow differs from the rheological response observed in shear mode. Yield hardening in flow mode is dominated by a densification process, which, in turn, depends on the initial volume fraction of particles in the fluid. In general, understanding the effect of the particle volume fraction on the response of ER fluids has proven to be challenging. For a given electric field, a linear dependence of the yield stress with an increasing particle volume fraction has been observed [18–20]. However, at higher-volume fractions, some report the presence of a maximum in the yield stress [18,19], while others observe an exponential-like growth [20]. A first step to resolve this discrepancy is to perform a systematic study comparing the effects of the particle volume fraction on the response of the ER fluid in the two different flow modes.

In the present study, we take this first step by experimentally investigating the yielding properties of ER fluids with different particle volume fractions under both steady simple shear flow and pressure-driven channel flow with a constant electric field. Values of Bingham yield stress are extracted from the data by regression to Eq. (1), and a comparison between the fluid responses in these two modes can then be performed. Finally, we present a model that captures the experimentally observed dependence of the fluid rheology on particle volume fraction in shear, as well as a phenomenological model that rationalizes the densification process and consequent yield hardening measured in channel flow. Our interest lies in using these densification models to predict the yield pressure of rapidly actuated hydraulic devices such as ER valves from viscometric measurements performed on a torsional rheometer.

II. MATERIALS AND METHODS

ER fluids with different particle volume fractions $(0 \le \phi \le 0.55)$ are prepared from a stock solution of a commercially available ER fluid (Fludicon, RheOil4). The stock solution has a particle volume fraction $\phi = 0.41$ and is made of a colloidal suspension of polyurethane (PUR) particles doped with Li^+ (mean diameter of 1.4 ± 0.6 μm) with silicone oil as a carrier fluid [21–23]. A SEM showing the morphology of the ER particles is shown in Appendix A. This class of ER fluids containing polymer particles doped with salt and/or polar organic dopants has been shown to exhibit a low base viscosity and a relatively high yield stress while having low current density. In addition, they also show good sedimentation and redispersion properties, a short response time (1–10 ms), and long-term stability making them a promising candidate for practical applications using electrorheological fluids [13,24]. Particle volume fractions lower than the stock solution are obtained by dilution with 100 cSt silicone oil while higher particle volume fractions are obtained by centrifuging the stock solution and removing a known volume of carrier fluid using a micropipette and then resuspending the centrifugate using an ultrasonic bath.

The rheological response of the ER fluid under shear mode is measured using an AR1000N stress-controlled rotational rheometer with a custom-made ER fixture which applies a uniform electric field between two aligned parallel plates. Steady-shear flow tests with decreasing shear rates varying from $4 \ge \dot{\gamma} \ge 0.1$ s^{-1} are performed using a parallel-plate geometry with a gap of 300 μm. This procedure analogous to that described by Ref. [25] is shown to ensure that a reproducible value of the dynamic yield stress is reached at steady state for a similar class of materials. The maximum shear rate applied is chosen as $\dot{\gamma} \le 4$ s^{-1} to minimize formation of shear-induced lamellar structures during the steady-shear flow tests that tend to be associated with a nonmonotonic flow curve [7,8]. This protocol ensures that the ER fluid remains homogeneous during the steady-shear flow tests and that modeling using the Bingham model [Eq. (1)] as well as comparison to flow data obtained from microchannels is applicable. The tests are performed at constant temperature $T = 22\,°C$ and constant particle volume fraction $\phi = 0.41$ with different electric fields as well as constant electric field $E = 3$ kV/mm for fluids with different particle volume fractions. The electric field $E = 3$ kV/mm is chosen

because it is of particular interest in valve applications: This electric field is high enough for potential engineering applications and for dielectrophoretic effects to be negligible and low enough to avoid electrical breakdown if an air bubble passes through the microchannel.

To measure the rheological response under flow mode, a rectangular microchannel is fabricated [17] (shown in Fig. 1). The microchannel consists of three regions: a test section with electrically conductive side walls through which the field is applied and two auxiliary sections with nonconductive side walls at the inlet and outlet to minimize effects due to the curvature of the streamlines. The two electrode side walls are made out of a conductive copper film (250 μm thick, 10 mm long) and separated by a 250-μm gap. For the nonconductive walls, a polyether ether ketone film of similar dimensions is used. To seal the microchannel, a 50-μm-thick adhesive film (3M, 966) bonded the films to a 1-mm-thick glass slide and a 3-mm-thick acrylic sheet with tapped holes for the inlet and outlet adapters. The portion of the microchannel, over which an electric field can be applied, has the dimensions $L = 10$ mm, $W = 350$ μm, $h = 250$ μm. The conductive side walls are connected to a high-voltage power supply (Stanford Research Systems PS350) via a driver circuit board. ER fluids are injected into the channel using a gastight glass syringe (Hamilton, 1005 TLL) that is connected to the microchannel with stainless-steel tubing (i.d. of 1.6 mm). The flow rate Q of the fluid is controlled by a syringe pump (Harvard Apparatus, PHD Ultra) and operated within the range of $30 \leq Q \leq 60$ μL/ min. The

pressure drop between the entry and exit of the channel is measured using a differential pressure sensor (Honeywell, 26PCBFA6D) with a measurement range of $0 \leq \Delta P \leq 35$ kPa; the signal is amplified and acquired using a DAQ board (National Instrument, DAQ1200). In the microchannel, gravity plays a negligible role, and the settling of the particles can be neglected. A lower bound on the characteristic time scale for settling is given by $t_{\text{settling}} \sim \mu h/(\rho_p - \rho_f)ga^2$ where a is the average particle diameter, and ρ_p, ρ_f are the densities of the particles and the fluid, respectively. We estimate $t_{\text{settling}} \sim 5000$ s, which is much larger than the time scales in our study, and therefore, settling can be considered negligible.

III. RESULTS AND DISCUSSION

Flow curves of the measured shear stress vs imposed shear rate curves for the stock solution ($\phi = 0.41$) at different electric fields obtained in shear mode are presented in Fig. 2, and the data are fit with the Bingham model [Eq. (1)]. We observe that in the absence of an electric field, the ER fluid behaves like a Newtonian fluid of viscosity $\mu = 31$ mPa s. When an electric field is applied for $E \geq 1.5$ kV/mm, the ER fluid develops a field-dependent yield stress as shown in Fig. 2(b).

The flow curves for the solutions with different particle volume fractions at $E = 3$ kV/mm obtained in shear mode are presented in Fig. 3. This data were fit with the Bingham model of Eq. (1). While some applications operate at high shear rates with an electric field applied (e.g., dampers and vibration control devices), for valve applications, our interest lies solely in the yield pressure of the valve and, thus, in the shear yield stress extracted from the Bingham model fit. For each volume fraction, the Bingham yield stress is extracted from the fit to be compared to the yield stress obtained from flow-mode measurements. Figure 4 shows a sample output for the pressure drop measured in a flow-mode experiment as a function of time at two different particle volume fractions ($\phi = 0.05, 0.4$) with an imposed flow rate $Q = 50$ μL/ min. The observed curves all indicate an initial pressure rise followed by a series of oscillations. At the beginning of each test, the electric field is activated causing the ER fluid initially present in the microchannel to block the flow. As the syringe pump displaces the fluid, the effective "lumped" compressibility $\beta = \frac{1}{V}\left(\frac{\Delta V}{\Delta P}\right)_T$ of the entire microfluidic system (consisting of the syringe, tubing, channel, and fluid contained therein) comes into play, and the pressure rises. For a given flow rate, the slope of the pressure rise is the same for different volume fractions and can be used to estimate this lumped compressibility β of the system ($\Delta P = -1/\beta \ln(1 - Qt/V_0)$ where V_0 is the volume of the system, $\beta = 5$ MPa^{-1}). When the imposed pressure difference exceeds a critical value, the ER microstructure yields, enabling the ER suspension to flow, thereby resulting in a drop in pressure. Since the
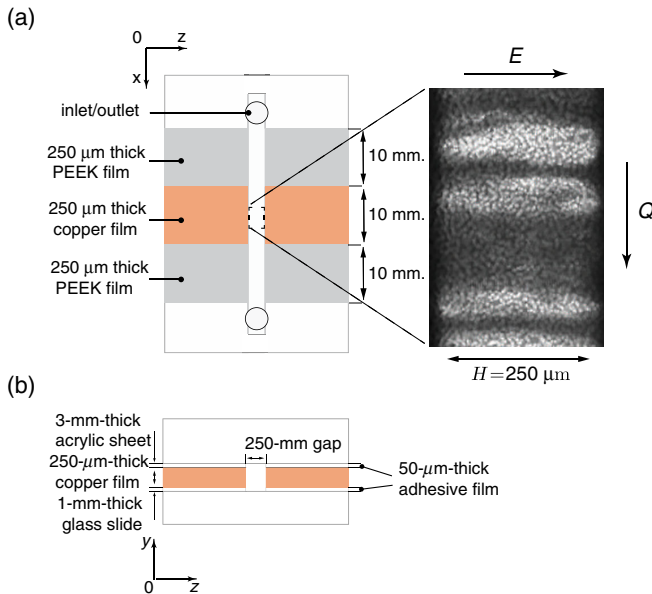
(a)

(b)

FIG. 1.   (a) Schematic top view of a microchannel fabricated for pressure measurements in flow mode. Also shown is a micrograph showing the microstructures that develop upon application of an electric field $E = 4$ kV/mm for $\phi_0 = 0.02$ (b) Cross-sectional view of the microchannel in the flow direction.
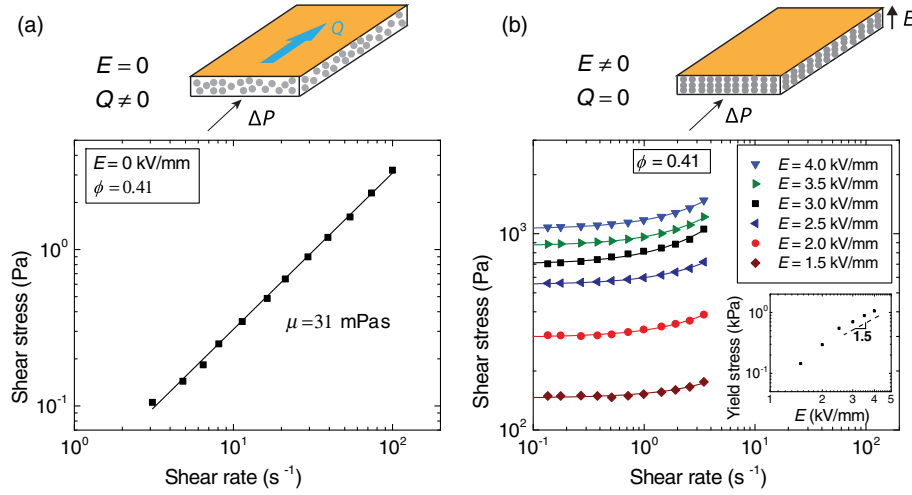
FIG. 2. Shear stress vs shear rate curves for different electric fields obtained from steady-shear flow tests on the AR1000N rheometer with a custom ER parallel-plate fixture ($R = 20$ mm, $H = 0.3$ mm) for $\phi = 0.41$. The lines indicate fits of the data with the Bingham model [Eq. (1)]. (a) Field-off case ($E = 0$ kV/mm): The ER fluid is Newtonian and flows easily through the microchannel. (b) Field-on case ($E > 0$ kV/mm): The ER fluid has a field-dependent yield stress, and flow can occur only in the microchannel if the applied pressure drop exceeds the yield pressure drop.

electric field is still present in the channel, at a second critical pressure, the flow is arrested once more and the compression cycle starts again, hence, the observed oscillations. By averaging over a series of peaks, we obtain an average value of the yield pressure differential at yield for the channel at each imposed mass flow rate. In the lubrication limit ($L \gg h, W$), the field-dependent pressure difference at yield $\Delta P_y(E, \phi)$ can be related to the Bingham yield stress using the following relation obtained via a global force balance on the system [17,26]:

$$\Delta P_y(E, \phi) = \frac{2\tau_y L(h + W)}{hW}, \qquad (2)$$

where L is the length of the channel over which the field is applied, and h is the gap between the electrodes. Using this relation, we can compute the Bingham yield stress $\tau_y(E, \phi)$ from the measured yield pressure for each flow rate and particle volume fraction.

The yield stress data extracted from the tests in shear and flow modes are shown in Fig. 5 as a function of the particle

volume fraction. We observe that for all the flow rates tested, the yield stress computed in flow mode is a weak function of the flow rate but is consistently greater than the one extracted from the steady-shear experiments. In steady shear, the yield stress is found to increase linearly with the particle volume fraction at low-volume fractions and then more rapidly at higher-volume fractions. In channel flow, we observe that after an initial increase, the extracted yield stress reaches a plateau value above a composition of $\phi \approx 0.25$. This plateau intersects the yield curve obtained from shear tests at $\phi \approx 0.54$. Electrorheological fluids, as well as yield stress fluids, are prone to slip under shear [27,28], and control experiments are performed to confirm that the measurements taken represent a true yield of the material and that wall slip does not play a major role in our measurements. Steady-shear flow tests performed on the
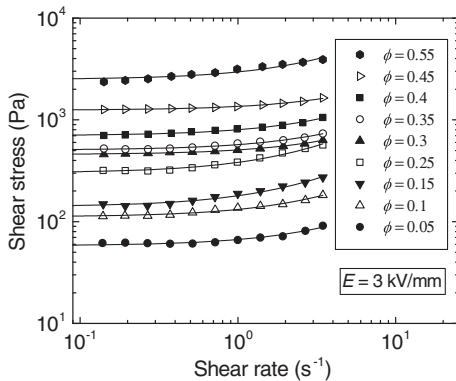

FIG. 3. Shear stress vs shear rate curves for different particle volume fractions obtained from steady-shear flow tests on the AR1000N rheometer with a custom ER parallel-plate fixture ($R = 20$ mm, $H = 0.3$ mm) at $E = 3$ kV/mm. The lines indicate select fits of the data with the Bingham model [Eq. (1)].
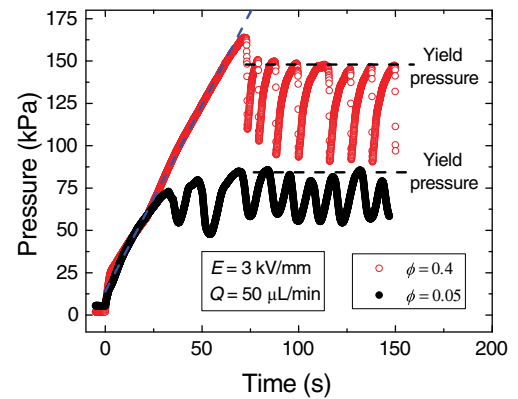

FIG. 4. Pressure drop across the microchannel for two different particle volume fractions ($\phi = 0.05, 0.4$) as a function of time for an electric field of $E = 3$ kV/mm and an imposed flow rate $Q = 50\ \mu$L/min. The dashed lines represent the peaks of the curve which are averaged to determine the yield pressure of the ER valve at each applied field strength, volumetric flow rate, and fluid volume fraction. The overall system compressibility is estimated from the slope (blue dotted line) of the pressure rise $\Delta P = -1/\beta \ln(1 - Qt/V_0)$, where V_0 is the volume of the system, $\beta = 5$ MPa^{-1}.
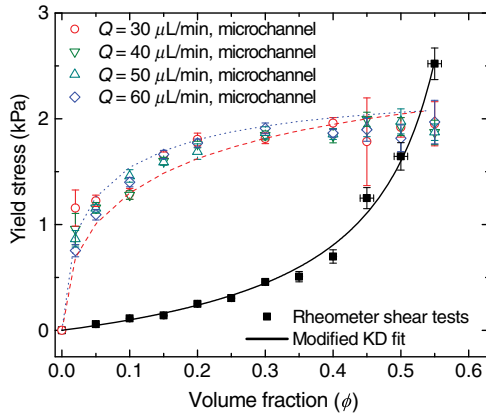
FIG. 5. Comparison of the yield stress extracted from the viscometric tests in the rheometer (Fig. 3) and from the yield pressure in the microchannel flow setup [Fig. 4 and Eq. (2)] for flow rates Q ranging from 30 to 60 μL/min as a function of the particle volume fraction for $E = 3$ kV/mm. The black solid line shows the fit of the modified Krieger-Dougherty (KD) model [Eq. (4)] to the viscometric data. The red and blue dashed lines show the fit of the proposed model obtained by combining Eqs. (4) and (7) with the microchannel data for $Q = 30$ and 60 μL/min, respectively.

rheometer are performed at different gaps [29] and are shown to superimpose for $\phi = 0.41$ and $E = 3$ kV/mm (Fig. 9 in Appendix C) indicating that wall slip plays a negligible role in our measurements for the range of the shear rates tested. For the case of channel flow, Video 1 in Appendix C taken using the imaging setup described by Qian *et al.* [17] demonstrates the absence of slip at the walls for a low-volume fraction fluid ($\phi = 0.02$) at an applied of field of $E = 4$ kV/mm and an imposed flow rate $Q = 30$ μL/min.

To rationalize these results, we note that in the steady-shear experiments, the system is closed, and the volume fraction of particles in the sample is fixed, whereas in channel flow, the system is open, and new particles are continuously convected into the microchannel, thus, potentially increasing the local volume fraction if the fluid exiting the channel is depleted in particles. Since the yield strength of the ER fluid is determined by its microstructure, which, in turn, depends on the local volume fraction of particles, the higher value of yield stress observed in channel flow and the saturation of the yield stress at higher-volume fractions are both consistent with an increase of the local volume fraction in the channel to a maximum value of $\phi_M \approx 0.54$. These results are consistent with the densification process described qualitatively by Nam *et al.* [15]. Optical transmissivity measurements performed by Qian *et al.* [17] show cluster formation in pressure-driven flow and the formation of a compaction front at the entrance of the microchannel that is associated with an increase in volume fraction. In addition, images taken by Tang *et al.* [8] show that after densification, at sufficiently high pressures, fingers appear near the inlet as the material

yields. This behavior is reminiscent of fluidization in jammed granular media [30] where compaction fronts and finger formation at sufficiently high pressures are known to occur. In granular systems where the interstitial fluid is compressible, e.g., air, diffusive propagation of the overpressure can play a role in the compaction process. However, in our system, the fluid is incompressible and such effects do not play a significant role in the dynamics of the system.

A. Modeling the yield stress in wall-driven shear flow

In a wall-driven shear flow with a homogeneous orthogonal electric field, the measured yield stress is a material function that depends solely on the electric field and the volume fraction of particles. Our focus is to model the effect of the volume fraction of particles on the yield stress of ER fluids in wall-driven flows.

Previous studies have shown that the yield stress of ER fluid in wall-driven shear flow exhibits a maximum [18,19], while others show a monotonic increase of the yield stress with volume fraction [31–33]. In our case, no maximum in yield stress is observed within the range of volume fractions studied. Based on the chain model, the influence of the particle volume fraction on the yield stress of ER fluids is often described using a power law or exponential model over the volume fractions studied [19,20,34]. These models fail to capture the effects observed here, namely, a linear dependence at low-volume fractions and a diverging behavior as the volume fraction approaches the maximum packing fraction (expected to be $\phi = 0.64$ for a random close packing of spherical monodisperse particles). The observed results are more akin to results obtained for concentrated suspensions of solid particles in yield stress fluids. For such suspensions, the viscometric properties (viscosity, shear modulus, yield stress) are often modeled using an empirical Krieger-Dougherty model [35–37]:

$$\frac{\tau_y(\phi)}{\tau_0} = \left(1 - \frac{\phi}{\phi_m}\right)^{-K\phi_m}, \tag{3}$$

where K is a coefficient that quantifies the initial linear increase in yield stress at low-volume fractions, τ_0 is a characteristic yield stress, and ϕ_m is the maximum packing fraction. K is analogous to the Einstein coefficient or intrinsic viscosity when the shear viscosity of a suspension is fitted to this model. We propose to model the influence of the particle volume fraction on the yield stress of the ER fluid by using a modified form of this relationship to account for the absence of a yield stress when no particles are present ($\phi = 0$):

$$\frac{\tau_y(\phi, E)}{\tau_0(E)} = \left[\left(1 - \frac{\phi}{\phi_m}\right)^{-K\phi_m} - 1\right]. \tag{4}$$

In this model, $\tau_0(E)$ is a characteristic field-dependent yield stress that reflects the strength of the attractive interaction between the particles. K is expected to be independent of

the electrical field E for $E \geq 1.5$ kV/mm where dielectrophoretic effects are negligible. As the field E increases, it is expected that the structures that form remain structurally similar, while the strength of the attractive interaction increases, leading to an increase of $\tau_0(E)$. A fit of this model to the yield stress in the shear vs volume fraction curve is shown in Fig. 5, and the coefficient of determination is found to be $R^2 = 0.98$ for $K = 1.23$, $\tau_0(E = 3$ kV/mm$) = 700$ Pa, and $\phi_m = 0.63$. A similar model was used by Mueller et al. [38] and Heymann et al. [39] to fit the yield stress of suspensions of solid spheres with $K\phi_m = 2$. We expect that this divergence from the case of solid suspensions is due to the fact that ER fluids are active materials that do not exhibit a yield stress in the absence of an electric field but rather develop this property through the aggregation of particles into chains and columns [4,15] and can form ordered lamellar structures upon the application of the electric field [7,8].

B. Modeling the yield stress in channel flow

As discussed, ER fluid flow in a channel is characterized by a densification process that is manifested as an increase in the local volume fraction of particles in the channel and in the overall pressure differential. Unlike wall-driven flow, the measured yield function is not a material property of the fluid but rather a complex function of the fluid and channel properties. Consider an ER fluid of initial volume fraction ϕ_0 that is pumped at a constant flow rate Q into an ER valve that is activated with a constant transverse-electric field E. Because of the electrostatic interactions, stable microstructures are formed in the channel through chaining and aggregation of particles. Eventually, these particulate chains may span the channel width and then become immobilized in the channel while the suspending solvent continues to flow out of the channel exit. The evolution of the structures formed during flow and, thus, the particle volume fraction in the channel is a complex function of ϕ_0, Q, and E.

We characterize the structures formed in the ER channel using the concept of hydraulic permeability κ which must satisfy the following conditions as shown in Fig. 6.
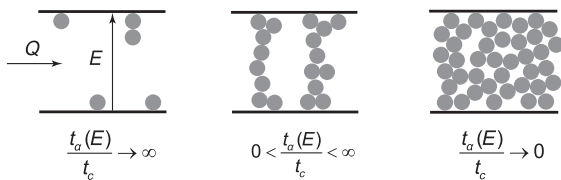

FIG. 6. Schematic of the chained microstructures built in the channel as a function of the nondimensional ratio of the aggregation time $t_\alpha(E)$ to the convective time $t_c(Q, \phi_0) = (LA/Q)[(\phi_M - \phi_0)/\phi_0]$. As the ratio $t_\alpha(E)/t_c(Q, \phi_0)$ gets smaller, the residence time in the channel becomes longer, there is less frustration, and the structures can anneal to a higher packing fraction ϕ_M.

First, at large flow rates $Q \to \infty$ or small initial volume fraction $\phi_0 \to 0$, all structures are unstable as the hydrodynamic forces acting on the chains dominate over the electrostatic forces. We expect no particles to be retained in the channel and, thus, a flow mobility $M_0 = (QL/Wh\Delta P)$ that is given by standard equations for viscous flow in a channel. Under the lubrication approximation $W \gg h$, $M_0 = (h^2/12\mu)$ where h is the electrode thickness (which forms the channel separation), W the width of the channel, and μ the viscosity of the fluid. The flow mobility can be related to an effective permeability κ_0 via the Darcy equation for flow in porous media, and we can define the permeability in this limit as $\kappa_0 = M_0\mu$. Second, in the limit $Q \to 0$, hydrodynamic forces are small, the particles reach a maximum packing volume fraction ϕ_M, and the chained microstructure that is formed by the ER suspension has a permeability κ_M. We note that the structure formed under dynamic flow conditions may be trapped at a maximum packing volume fraction ϕ_M that is lower than the maximum possible packing fraction reached under static conditions ϕ_m. These conditions are in agreement with the experimental observations of Tang et al. [8] and Nam et al. [15] that show that cluster size observed in channel flow decreases with the imposed flow rate. The existence of several time scales in the evolution of the structure of ER fluids has been shown in previous reports [8,15,17,40,41]: a short time scale related to the aggregation of particles into chains and a longer time scale associated with cluster formation. Following the work by Qian et al. [17], the electric field sets a time scale for aggregation $t_\alpha(E)$, while the structure formation is governed by the ratio of the convective time scale for the flowing suspension t_c to the aggregation time scale $t_\alpha(E)$. The convective time scale $t_c(Q, \phi_0)$ is given by $t_c(Q, \phi_0) = (LA/Q)[(\phi_M - \phi_0)/\phi_0]$ and represents the time needed to fill a channel of length L and cross section A to the maximum volume fraction ϕ_M when starting from an initial volume fraction ϕ_0.

We propose the following permeability function κ_s that defines the overall microstructure formed within the channel:

$$\kappa_s = \kappa_M + (\kappa_0 - \kappa_M)(1 - e^{-[t_\alpha(E)/t_c(Q,\phi_0)]}). \quad (5)$$

This function satisfies the experimental observations described above and physically corresponds to the fact that under fast flow rates or small initial volume fractions, the structure formed will be more permeable than at slow flow rates. As the flow rate is reduced, the suspended particles have more time to rearrange and reach the maximum packing fraction ϕ_M without getting trapped in a frustrated or jammed state at a lower-volume fraction. An analogous functional form was proposed by Nakano et al. [16] to model the dependence of the

pressure drop for flow of ER fluids in a rectangular channel on the flow rate and shown to agree with their experimental results.

To relate permeability and average volume fraction in the channel at any given time, we use the simple relation proposed by Qian et al. [17]

$$\kappa = \kappa_0 (1 - \phi)^n, \qquad (6)$$

where ϕ is the average volume fraction in the channel, and n is an empirical parameter found to be $n = 6$ by Qian et al. [17]. This functional form is chosen because it was shown experimentally using light intensity measurements that it provides a good approximation to the evolution of the permeability in an ER channel. In addition, it is readily invertible, thus, providing an exact expression for the average volume fraction of particles in the channel for a given permeability. A more in-depth discussion comparing permeability models from the literature and this model is provided in Appendix B. Combining Eqs. (5) and (6), we can compute the average volume fraction ϕ_s of the assembled microstructures built in the channel during shear flow:

$$\phi_s(E, Q, \phi_0) = 1 - \left[\frac{\kappa_M}{\kappa_0} + \left(1 - \frac{\kappa_M}{\kappa_0}\right)\left(1 - e^{-[t_\alpha(E)/t_c(Q,\phi_0)]}\right)\right]^{1/n}.$$

$$(7)$$

By combining Eqs. (4) and (7), the yield stress of the permeable microstructure that assembles in the channel is then given by $\tau_y(\phi_s)$, where $\tau_y(\phi)$ is the material function that is measured independently under wall-driven shear flow in the rheometer and discussed earlier in Eq. (4).

Figure 5 shows the experimental data and the model predictions of the yield stress in our channel geometry obtained by combining Eqs. (4) and (7) for $t_\alpha(E) =$ 3.5 ms and a maximum packing fraction $\phi_M = 0.54$ for two different flow rates: 30 and 60 μL/ min. The model demonstrates the ability to capture the experimental observation discussed earlier for ER fluids in pressure-driven microchannel flow: a sharp increase of the yield stress at low initial volume fractions, followed by saturation at high initial volume fractions and a weak dependence of the measured results on the flow rate. The fitted value found for the aggregation time scale $t_\alpha(E) = 3.5$ ms is within the range reported in the literature for electrorheological fluids [5,13,15,19]. The analysis performed does not depend sensitively on the choice of the permeability model, provided the permeability of the chained microstructure in the channel is a monotonically decreasing function of the particle volume fraction (as is expected). This simple two-parameter phenomenological model, thus, offers a simple, yet rich, physical mechanism to model the yield hardening observed in channel flow. Previous work has focused on showing that each mode of shear must be characterized by separate experiments to model the performance of ER fluids in devices of interest. Using our model and the physical understanding of the densification that occurs in channel flow, we demonstrate that we are able to model and predict the rheological performance in channel flow using an independent characterization of the dependence of the yield stress on the particle volume fraction performed in wall-driven flow [Eq. (4)]. This allows us to reconcile the discrepancies observed in the two modes of flow.

IV. CONCLUSIONS

When designing devices using active suspensions in flow mode, the phenomenon of yield hardening must be considered. Specifically, the local densification in the microstructure must be taken into account in the systems modeling, since it controls the magnitude of the yield pressure in the device. In the present work, we show that the complex interdependencies between the electrostatic interactions, the hydrodynamic forces, and the channel geometry can be modeled by understanding the ratio of the particle aggregation time scale to the convective flow time scale and linked to the permeability of the chained microstructures that assemble in the channel when a transverse-electric field is applied to the flow. The understanding of flow-induced densification and saturation is important in optimizing parameters such as channel length and switching time in ER-fluidic valve design. With the physical understanding of the densification that occurs in channel flow, we can model and predict the performance in channel flow using a characterization of the dependence of the yield stress on the particle volume fraction performed in wall-driven flow, thus, allowing us to reconcile the discrepancies observed in the two modes of flow.

APPENDIX A: MORPHOLOGY OF THE ER PARTICLES

The morphology and size distribution of the ER particles present in RheOil 4.0 are shown in Fig. 7. The mean diameter is $d = 1.4 \pm 0.6$ μm.
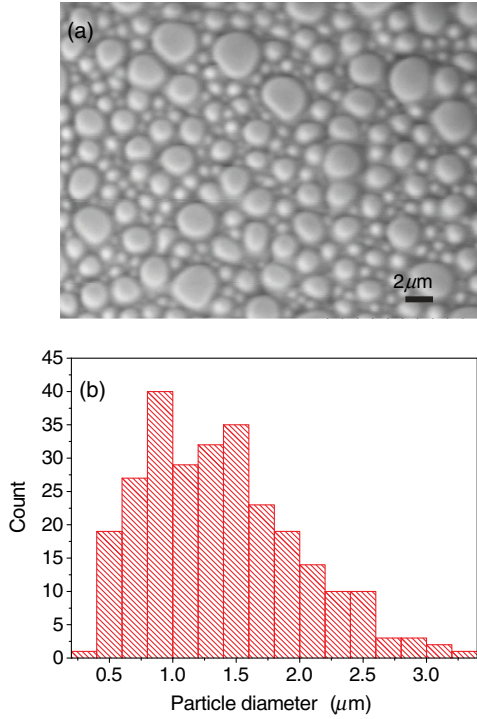
FIG. 7. Morphology of ER particles. (a) SEM image showing the morphology of the polyurethane particles contained in the ER fluid. (b) Histogram of particle-size distribution in the ER fluid.

APPENDIX B: COMPARISON OF PERMEABILITY MODELS

In this section, we discuss the sensitivity of our densification model to the choice of the permeability model. As suspended particles flow into the channel, chainlike microstructures are built dynamically, first forming chains then coarsening them [18,19]. Because of the complex dynamic nature of this process, it is difficult to make a comparison to traditional permeability models in porous media that are based on a preexisting static structure. Nonetheless, we compare in this section the model used by Qian *et al.* [17] to permeability models from the porous media literature that characterize flow past an array of cylinders [17,19], despite the fact that in our system, a wide range of different column sizes form during flow and assembly, we make the comparison of our chosen model [17] to models with an array of columns of fixed diameter d (Ergun [42] and Tamayol and Bahrami [43]). Physically, this corresponds to approximating flow in the channels to flow through the largest pores or structures in our structures that have an average diameter size on the order of d.

The total hydraulic resistance in a microfluidic channel partially filled with ER particles can be modeled as the open channel and the chained microstructures in series, and, thus, the overall permeability is given by $\kappa = [\kappa_p \kappa_0 / (\kappa_p + \kappa_0)]$ where κ_0 is the open-channel permeability and κ_p the permeability of the static microstructure.
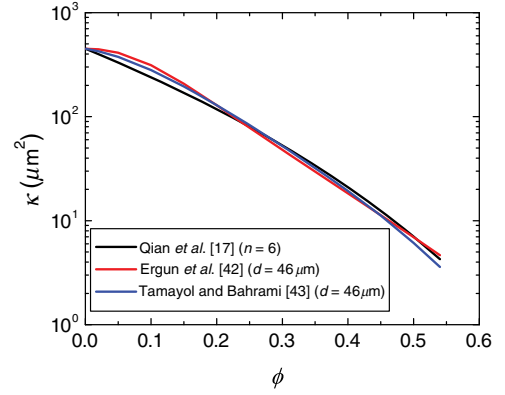

FIG. 8. Comparison of the overall system permeability predicted by Qian *et al.* [17] with $\kappa_0 = 4.5 \times 10^2$ μm^2 and $n = 6$, Ergun *et al.* [42] and Tamayol and Bahrami [43]. For $d = 46$ μm, the permeability is predicted to be very similar for all three models.

The expressions for κ_p for the different models are given below,

$$\kappa_{p,\text{Ergun}} = \frac{d^2}{150} \frac{(1 - \phi)^3}{\phi^2}, \tag{B1}$$

$$\kappa_{p,\text{Tamayol}} = 0.16 \alpha d^2 \frac{\left(1 - \sqrt{\frac{\phi}{\alpha}}\right)^3}{\phi \sqrt{1 - \phi}}, \tag{B2}$$

where $\alpha = (\pi/4)$ is for a square packing of cylinders and $\alpha = (\pi/2\sqrt{3})$ is for a hexagonal packing. We note that the model proposed by Ergun *et al.* [42] has the same functional dependence on volume fraction as the Carman-Kozeny classical relation for a random packing of spheres [44,45].

We compare the overall permeability given by these models to the simple expression given by Qian *et al.* [17] $\kappa = \kappa_0 (1 - \phi)^n$ where κ_0 is the open-channel permeability $(\kappa_0 = 4.5 \times 10^2$ $\mu m^2)$, and n is an empirical parameter found to be $n = 6$. As shown in Fig. 8, the permeability predicted by the different models is in good agreement for an average column diameter $d = 46$ μm. This size is reasonable for the typical length scale of the structures in the channel, as the particles (with an average diameter of 2.5 μm) are convected into the channel and jam dynamically under flow.

APPENDIX C: IMPORTANCE OF WALL SLIP IN VISCOMETRIC AND CHANNEL FLOW MEASUREMENTS

Yield stress fluids including ER fluids, particularly at high particle volume fractions, are prone to wall slip during viscometric and channel flow. To correct for slip in the parallel-plate geometry on the rheometer, the protocol proposed by Yoshimura and Prud'homme [29] is followed.
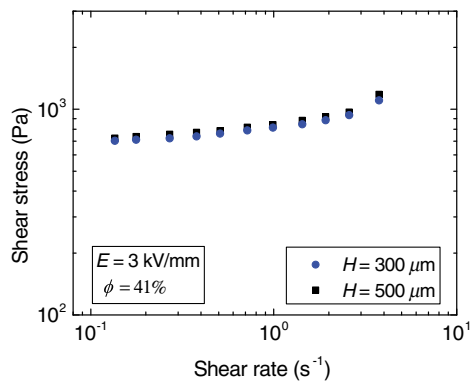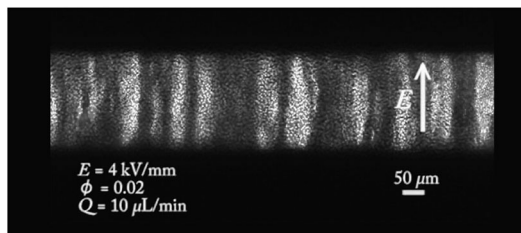
FIG. 9.   Shear stress vs shear rate curves for different rheometer gaps obtained from steady-shear flow tests on the AR1000N rheometer with a custom ER parallel-plate fixture ($R = 20$ mm) for $\phi = 0.41$ and $E = 3$ kV/mm. The flow curves obtained at different gaps superimpose, showing that wall slip plays a negligible role in the steady-shear flow tests performed on the rheometer.

VIDEO 1.   Video taken using the imaging setup described by Qian *et al.* [17] demonstrating the absence of slip at the walls for a low-volume fraction fluid ($\phi = 0.02$) at an applied of field of $E = 4$ kV/mm and an imposed flow rate $Q = 30$ μL/ min.

The sample is tested at two different gaps ($H = 0.5$ and 0.3 mm, respectively) to probe and correct for slip effects. If the flow curves at different gaps superimpose, then the wall slip is negligible. If gap-dependent rheology is observed, a correction needs to be applied to extract the true shear rate applied on the sample at each value of the applied stress. The flow curves for $\phi = 0.41$ and $E = 3$ kV/mm at two different gaps are shown in Fig. 9 and show that wall slip plays a negligible role in the steady-shear flow tests performed on the rheometer.

For the corresponding case of pressure-driven channel flow, Video 1 demonstrates the absence of slip at the walls for a low-volume fraction fluid ($\phi = 0.02$) at an applied field of $E = 4$ kV/mm and an imposed flow rate $Q = 30$ μL/ min.

[1] W. M. Winslow, Induced fibration of suspensions, J. Appl. Phys. **20**, 1137 (1949).

[2] R. Stanway and J. L. Sproston, Electro-rheological fluids: A systematic approach to classifying modes of operation, J. Dyn. Syst., Meas., Control **116**, 498 (1994).

[3] John P. Coulter, Keith D. Weiss, and J. David Carlson, Engineering applications of electrorheological materials, J. Intell. Mater. Syst. Struct. **4**, 248 (1993).

[4] Daniel J. Klingenberg and Charles F. Zukoski, Studies on the steady-shear behavior of electrorheological suspensions, Langmuir **6**, 15 (1990).

[5] Xize Niu, Weijia Wen, and Yi-Kuen Lee, Micro valves using nanoparticle-based giant electrorheological fluid, in *Proceedings of the 13th International Conference on Solid-State Sensors, Actuators and Microsystems, 2005* (IEEE, New York, 2005), Vol. 1, pp. 652–655.

[6] K. Yoshida, M. Kikuchi, J. H. Park, and S. Yokota, Fabrication of micro electro-rheological valves (ER valves) by micromachining and experiments, Sens. Actuators A **95**, 227 (2002).

[7] J. G. Cao, J. P. Huang, and L. W. Zhou, Structure of electrorheological fluids under an electric field and a shear flow: Experiment and computer simulation, J. Phys. Chem. B **110**, 11635 (2006).

[8] X. Tang, W. H. Li, X. J. Wang, and P. Q. Zhang, Structure evolution of electrorheological fluids under flow conditions, Int. J. Mod. Phys. B **13**, 1806 (1999).

[9] Yannis Pappas and Daniel J. Klingenberg, Simulations of magnetorheological suspensions in Poiseuille flow, Rheol. Acta **45**, 621 (2006).

[10] R. Tao, Super-strong magnetorheological fluids, J. Phys. Condens. Matter **13**, R979 (2001).

[11] Yu Tian, Xuli Zhu, Jile Jiang, Yonggang Meng, and Shizhu Wen, Structure factor of electrorheological fluids in compressive flow, Smart Mater. Struct. **19**, 105024 (2010).

[12] Ho Guen Lee and Seung Bok Choi, Dynamic properties of an ER fluid under shear and flow modes, Mater. Des. **23**, 69 (2002).

[13] M. Gurka, R. Petricevic, S. Schneider, and S. Ulrich, Characterization of step response time and bandwidth of electrorheological fluids, J. Intell. Mater. Syst. Struct. **22**, 1745 (2011).

[14] Y. J. Jang, M. S. Suh, M. S. Yeo, and S. B. Choi, The numerical analysis of channel flows of ER fluids, J. Intell. Mater. Syst. Struct. **7**, 604 (1996).

[15] Y. J. Nam, M. K. Park, and R. Yamane, Dynamic responses of electrorheological fluid in steady pressure flow, Exp. Fluids **44**, 915 (2008).

[16] Masami Nakano, Ryuji Aizawa, and Yoshinobu Asako, Steady and transient responses of electrorheological suspensions passing through a rectangular channel, Int. J. Mod. Phys. B **10**, 2965 (1996).

[17] Bian Qian, Gareth H. McKinley, and A. E. Hosoi, Structure evolution in electrorheological fluids flowing through microchannels, Soft Matter **9**, 2889 (2013).

[18] R. T. Bonnecaze and J. F. Brady, Yield stresses in electrorheological fluids, J. Rheol. **36**, 73 (1992).

[19] Tian Hao, *Electrorheological Fluids the Non-Aqueous Suspensions*, edited by B. V. Elsevier (Elsevier, New York, 2005), pp. 152–234.

[20] Zhenyang Song, Yuchuan Cheng, Jinghua Wu, Jianjun Guo, and Gaojie Xu, Influence of volume fraction on the yield behavior of giant electrorheological fluid, Appl. Phys. Lett. **101**, 101908 (2012).

[21] RheOil 4.0, ERF Production Würzburg GmbH Product Information on RheOil 4.0, http://www.erfgmbh.de.

[22] Yanina Reichert and Holger Böse, in *Electro-Rheological Fluids and Magneto-Rheological Suspensions*, edited by Rongjia Tao (World Scientific, Singapore, 2011), pp. 338–347.

[23] Steffen Schneider and S. Eibl, Review of the ER effect of polyurethane-based ER fluids, Applied Rheology **18**, 23956 (2008).

[24] M. Gurka, L. Johnston, and R. Petricevic, New electro-rheological fluids—Characteristics and implementation in industrial and mobile applications, J. Intell. Mater. Syst. Struct. **21**, 1531 (2010).

[25] G. Ovarlez, S. Cohen-Addad, K. Krishan, J. Goyon, and P. Coussot, On the existence of a simple yield stress fluid behavior, J. Non-Newtonian Fluid Mech. **193**, 68 (2013).

[26] R. B. Bird, R. C. Armstrong, and O. Hassager, *Dynamics of Polymeric Liquids*, 2nd ed. (John Wiley and Sons Inc., New York, 1987), Vol. 1.

[27] Steffen Schneider, Wall slip effects measuring the rheological behavior of electrorheological (ER) suspensions, Int. J. Mod. Phys. B **26**, 1250006 (2012).

[28] Richard Buscall, Letter to the Editor: Wall slip in dispersion rheometry, J. Rheol. **54**, 1177 (2010).

[29] Ann Yoshimura and Robert K. Prud'homme, Wall slip corrections for Couette disk viscometers and parallel disk viscometers, J. Rheol. **32**, 53 (1988).

[30] Johnsen Ø, C. Chevalier, A. Lindner, R. Toussaint, E. Clément, K. J. Måløy, E. G. Flekkøy, and J. Schmittbuhl, Decompaction and fluidization of a saturated and confined granular medium by injection of a viscous liquid or gas, Phys. Rev. E **78**, 051302 (2008).

[31] X. D. Pan and Gareth H. McKinley, Simultaneous measurement of viscoelasticity and electrical conductivity of an electrorheological fluid, Langmuir **14**, 985 (1998).

[32] C. J. Gow and C. F. Zukoski, The electrorheological properties of polyaniline suspensions, J. Colloid Interface Sci. **136**, 175 (1990).

[33] Louise Marshall, Charles F. Zukoski, and James W. Goodwin, Effects of electric fields on the rheology of non-aqueous concentrated suspensions, J. Chem. Soc., Faraday Trans. 1 **85**, 2785 (1989).

[34] K. P. S. Parmar, Y. Méheust, Børge Schjelderupsen, and J. O. Fossum, Electrorheological suspensions of laponite in oil: Rheometry studies, Langmuir **24**, 1814 (2008).

[35] Irvin M. Krieger and Thomas J. Dougherty, A mechanism for non-Newtonian flow in suspensions of rigid spheres, Trans. Soc. Rheol. **3**, 137 (1959).

[36] Xavier Chateau, Guillaume Ovarlez, and Kien Luu Trung, Homogenization approach to the behavior of suspensions of noncolloidal particles in yield stress fluids, J. Rheol. **52**, 489 (2008).

[37] Michael Kogan, Lucie Ducloué, Julie Goyon, Xavier Chateau, Olivier Pitois, and Guillaume Ovarlez, Mixtures of foam and paste: Suspensions of bubbles in yield stress fluids, Rheol. Acta **52**, 237 (2013).

[38] S. Mueller, E. W. Llewellin, and H. M. Mader, The rheology of suspensions of solid particles, Proc. R. Soc. A **466**, 1201 (2010).

[39] Lutz Heymann, Sigrid Peukert, and Nuri Aksel, On the solid-liquid transition of concentrated suspensions in transient shear flow, Rheol. Acta **41**, 307 (2002).

[40] B. Abu-Jdayil, Response time of an ER-fluid under shear and flow modes, J. Phys. Conf. Ser. **412**, 012009 (2013).

[41] J. C. Hill and T. H. Van Steenkiste, Response times of electrorheological fluids, J. Appl. Phys. **70**, 1207 (1991).

[42] S. Ergun, Fluid flow through packed columns, Chem. Eng. Prog. **48**, 89 (1952).

[43] Ali Tamayol and Majid Bahrami, Transverse permeability of fibrous porous media, Phys. Rev. E **83**, 046314 (2011).

[44] P. C. Carman, Fluid flow through granular beds, Trans. Inst. Chem. Eng. **15**, 150 (1937).

[45] J. Kozeny, Ueber kapillare Leitung des Wassers im Boden, Sitzungsber Akad. Wiss., Wien **136**, 271 (1927).